Onubogu *et al. EURASIP Journal on Wireless Communications and Networking* [redacted]
DOI 10.1186/s13638-015-0411-5

EURASIP Journal on Wireless Communications and Networking
a SpringerOpen Journal

RESEARCH Open Access

Experimental evaluation of the performance of 2×2 MIMO-OFDM for vehicle-to-infrastructure communications

Okechukwu J. Onubogu[1*], Karla Ziri-Castro[1], Dhammika Jayalath[1] and Hajime Suzuki[2]

Abstract

In this paper, a novel 2 × 2 multiple-input multiple-output orthogonal frequency division multiplexing (MIMO-OFDM) testbed based on an Analog Devices AD9361 highly integrated radio frequency (RF) agile transceiver was specifically implemented for the purpose of estimating and analyzing MIMO-OFDM channel capacity in vehicle-to-infrastructure (V2I) environments using the 920 MHz industrial, scientific, and medical (ISM) band. We implemented two-dimensional discrete cosine transform-based filtering to reduce the channel estimation errors and show its effectiveness on our measurement results. We have also analyzed the effects of channel estimation error on the MIMO channel capacity by simulation. Three different scenarios of subcarrier spacing were investigated which correspond to IEEE 802.11p, Long-Term Evolution (LTE), and Digital Video Broadcasting Terrestrial (DVB-T)(2k) standards. An extensive MIMO-OFDM V2I channel measurement campaign was performed in a suburban environment. Analysis of the measured MIMO channel capacity results as a function of the transmitter-to-receiver (TX-RX) separation distance up to 250 m shows that the variance of the MIMO channel capacity is larger for the near-range line-of-sight (LOS) scenarios than for the long-range non-LOS cases, using a fixed receiver signal-to-noise ratio (SNR) criterion. We observed that the largest capacity values were achieved at LOS propagation despite the common assumption of a degenerated MIMO channel in LOS. We consider that this is due to the large angular spacing between MIMO subchannels which occurs when the receiver vehicle rooftop antennas pass by the fixed transmitter antennas at close range, causing MIMO subchannels to be orthogonal. In addition, analysis on the effects of different subcarrier spacings on MIMO-OFDM channel capacity showed negligible differences in mean channel capacity for the subcarrier spacing range investigated. Measured channels described in this paper are available on request.

Keywords: MIMO-OFDM; Capacity; V2I; LOS; Channel

1 Review

1.1 Introduction

Multiple-input multiple-output (MIMO) systems have attracted considerable attention due to the increasing requirements of high capacity, spectral efficiency, and reliability in wireless communications. For example, MIMO systems have been adopted in the Long-Term Evolution (LTE) system, and it is expected that the upcoming developments in IEEE 802.11p and Digital Video Broadcasting Terrestrial (DVB-T) wireless standards will include the use of MIMO. It has been shown [1] that MIMO, when deployed in a rich scattering environment, is capable of achieving high spectral efficiency, capacity, and reliability by exploiting the increased spatial degrees of freedom. MIMO is often combined with the orthogonal frequency division multiplexing (OFDM) in modern wireless standards in order to achieve higher data rates and performance improvements in a multipath fading environment without increasing the required bandwidth or transmission power.

Efficient vehicular communication is a key in the development of intelligent transport systems (ITS) and requires the exchange of messages between two vehicles (vehicle-to-vehicle or V2V communications) or between a vehicle and a roadside unit (vehicle-to-infrastructure or V2I com-

*Correspondence: okechukwu.onubogu@qut.edu.au
[1] School of Electrical Engineering and Computer Science, Queensland University of Technology, Brisbane, QLD 4001, Australia
Full list of author information is available at the end of the article

munications). Basically, there are two kinds of vehicular applications: those dedicated to providing safety services and others for non-safety applications [2]. For safety purposes, the use of licensed band at 5.9 GHz has been considered to avoid the problem of interference typically faced in the use of industrial, scientific, and medical (ISM) radio bands. Non-safety applications use the ISM band for the purpose of infotainment (e.g., high data rate Internet access for video streaming) where the availability of the service is expected to be opportunistic. The 920 MHz ISM band in Australia occupies 918–926 MHz. Among the ISM bands, the 920 MHz band gives an optimal tradeoff of robustness against slow fading, achieving a longer range in cluttered environments and having a sufficient bandwidth for the high-data-rate Internet access. This paper focuses on the non-safety V2I applications at the 920 MHz ISM band which promises to provide infotainment applications, mobile internet services, and social network applications which are widely used in people's daily activities in vehicles. The successful deployment of commercial MIMO systems will require a solid understanding of the channel characteristics in which it will operate. In order to assess the performance of new wireless communication systems using MIMO antennas, it is desirable to evaluate them in realistic measurement scenarios. Consequently, numerous MIMO channel measurement campaigns have been carried out in vehicular environments [3–7]. However, only a few research publications have considered MIMO V2V channels [8–12], and even fewer theoretically based research works have investigated MIMO V2I channels [13, 14]. A number of single-input single-output (SISO) antenna V2V and V2I channel measurement campaigns have been conducted [15, 16]. However, to the best of our knowledge, we are not aware of any MIMO-OFDM measurement results for V2I communications published in the scientific literature to date. In this paper, we focus on presenting the results of an experimental investigation of 2×2 MIMO-OFDM channel measurements performed in a real V2I driving scenario under both line-of-sight (LOS) and non-LOS (NLOS) conditions at the 920 MHz ISM band in a suburban environment. A channel sounding system based on a software-defined radio (SDR) platform was implemented and used to perform an extensive measurement campaign in a suburban environment. In comparison to the use of the conventional heavy and expensive radio frequency (RF) test equipment such as signal generators, vector network analyzers, and spectrum analyzers, SDR provides a flexible, inexpensive, and cost-effective measurement setup implemented in software that enables researchers to use and control the radio signal through software tools such as MATLAB.

The rapid development of MIMO systems has been based on the assumption that independent and identically distributed (i.i.d) or correlated Rayleigh fading with NLOS components is available and a high number of multipath components are created by the surrounding environment [17–19]. This, however, is not valid in all cases, and it is violated due to the existence of a LOS component that is stronger than other components. Hence, the channel can be more effectively modeled using the Ricean distribution. Conventionally, the presence of a LOS component is thought to limit the benefits of MIMO systems because of the rank deficiency of the channel matrix [20, 21]; however, a number of investigations [13, 14, 22–26] have shown that using antennas positioned or spaced in such a way that the LOS MIMO subchannels are orthogonal results in a full-rank MIMO channel matrix and therefore high-capacity channels. The common idea behind these approaches is to place the antenna elements sufficiently far apart so that the spatial LOS MIMO subchannels become orthogonal with a phase difference of $\pi/2$. The optimal spacings can be worked out via simple geometrical tools, while the channel matrix becomes full rank and delivers equal eigenvalues. This is known as an optimized LOS MIMO system [24]. We can determine the required inter-element spacings to achieve the maximum 2×2 MIMO capacity. The formula is a function of the inter-element distance, the transmitter-to-receiver (TX-RX) separation distance, the orientation of the arrays, and the carrier frequency.

This paper validates the theoretical maximum LOS MIMO capacity criteria in [14, 25, 27, 28] by presenting a measurement-based analysis of mean MIMO capacity (mean over the channel bandwidth and the time of 50 ms) as a function of TX-RX separation distance. The technique is based on the achievement of spatial multiplexing in scenarios by creating an artificial multipath not caused by physical objects but rather by deliberate antenna placement or separation of the antenna elements in such a way that a deterministic and constant orthogonal multipath is created at a specific TX-RX separation distance called D_{opt}. This paper also analyzes the MIMO channel capacity for three different subcarrier spacings: large subcarrier spacing (LSS), medium subcarrier spacing (MSS), and small subcarrier spacing (SSS). These subcarrier spacings approximately correspond to IEEE 802.11p Wireless Access in Vehicular Environment, LTE, and the 2k version of the DVB-T standard. It is important to note that this paper analyzes the capacity of the MIMO channels with three different values of subcarrier spacing and not the capacity of the whole system. In this analysis, the MIMO channels are estimated by the least square (LS) channel estimation method with known channel training symbols [29]. The channel estimation error due to lower signal-to-noise ratio (SNR) at a longer TX-RX separation distance is substantially reduced by applying two-dimensional discrete cosine transform (2D DCT)-based

filtering to take advantage of the time and frequency coherence of the channel [30–32].

The remainder of the paper is organized as follows. Section 1.2 describes the channel model, MIMO channel capacity, the derivation for maximum LOS MIMO channel capacity criteria, and the LS channel estimation. Section 1.3 presents the MIMO-OFDM V2I measurement equipment, measurement environment, and parameters. In Section 1.4, we present the analysis of measurement results. Finally, Section 2 summarizes the paper and adds concluding remarks.

1.2 Channel model and capacity

1.2.1 LOS MIMO channel model

To investigate the capacity of a MIMO channel in the presence of a LOS component, a suitable channel model for the MIMO channel is needed. According to [21, 28] and [25], a suitable way to model the channel matrix is as a sum of two components, a LOS component and a NLOS component. The ratio between the power of the two components gives the Ricean K factor. The MIMO channel matrix is modeled as

$$\mathbf{H} = \sqrt{\frac{K}{K+1}}\mathbf{H}_{\text{LOS}} + \sqrt{\frac{1}{K+1}}\mathbf{H}_{\text{NLOS}} \tag{1}$$

where $\mathbf{H}_{\text{LOS}}$ denotes the matrix containing the free space responses between all elements, $\mathbf{H}_{\text{NLOS}}$ accounts for the scattered signals, and K is the Ricean K-factor which is equal to the ratio of the free space and scattered signals [33, 34]. As given in [25] and [27], the free space component, $\mathbf{H}_{\text{LOS}}$, of the complex response between a transmitting element m and a receiving element n (assuming that both elements are isotropic) is given as $e^{-j\beta d_{n,m}}/d_{n,m}$ where β is the wave number corresponding to the carrier wavelength λ and it is given as $\beta = \frac{2\pi}{\lambda}$. $d_{n,m}$ is the distance between the nth receiving element and the mth transmitting element. With the assumption that the difference in the pathloss is negligible and that there is no mutual coupling between the elements, the normalized free space response matrix of an $n_r \times n_t$ MIMO system can be expressed as

$$\mathbf{H}_{\text{LOS}} = \begin{bmatrix} e^{-j\beta d_{1,1}} & e^{-j\beta d_{1,2}} & \dots & e^{-j\beta d_{1,n_t}} \\ e^{-j\beta d_{2,1}} & e^{-j\beta d_{2,2}} & \dots & e^{-j\beta d_{2,n_t}} \\ \vdots & \vdots & \vdots & \ddots \\ e^{-j\beta d_{n_r,1}} & e^{-j\beta d_{n_r,2}} & \dots & e^{-j\beta d_{n_r,n_t}} \end{bmatrix}$$

where $\mathbf{H}_{\text{LOS}}$ is totally deterministic and depends only on the positioning or separation distance between both elements of the RX and TX antennas. Contrastingly, the response due to $\mathbf{H}_{\text{NLOS}}$ is a random complex matrix and is often modeled by stochastic process, i.e., $\mathbf{H}_{\text{NLOS}} \in \subset^{n_r \times n_t}$ with i.i.d elements.

1.2.2 MIMO channel capacity

In any communication system, the fundamental measure of performance is the capacity of the channel, which is the maximum rate of communication for which arbitrarily small error probability can be achieved [35]. In this section, the capacity definition of MIMO systems is presented and the minimum and maximum capacity criteria are derived in terms of the channel response matrix. In this case, the receiver is assumed to have perfect channel state information (CSI) but no such prior knowledge is available at the transmitter. Hence, the Shannon capacity formula for the MIMO channel is given as [1, 36]

$$C_k = \log_2\left(\det\left(\mathbf{I}_{n_r} + \frac{\rho}{n_t}\mathbf{H}_k\mathbf{H}_k^H\right)\right) \tag{2}$$

where C_k is the MIMO channel capacity in bits per second per Hertz (bits/s/Hz) at the kth OFDM subcarrier, $\mathbf{I}_{n_r}$ is the identity matrix and superscript H denotes the complex conjugate transpose (Hermitian), ρ corresponds to the average received SNR per receiver over MIMO subchannels, and n_t and n_r are the number of transmitting and receiving antenna elements, respectively. We note that the above capacity formula relies on a uniform power allocation scheme at all transmitting elements. Assuming that $n_t \leq n_r$, we can write

$$C_k = \sum_{m=1}^{n_t} \log_2\left(1 + \frac{\rho}{n_t}\gamma_m(\mathbf{H}_k)\right) \tag{3}$$

where $\gamma_m(\mathbf{H}_k)$ is the mth eigenvalue of $\mathbf{H}_k\mathbf{H}_k^H$. The maximum capacity is achieved when the channel is orthogonal [1], for which $\mathbf{H}_k\mathbf{H}_k^H$ is a diagonal matrix with $||\mathbf{H}_{k,m}||_F^2$ as its (m,m)-th element, where $||\mathbf{H}_{k,m}||_F^2$ is the squared Frobenius norm of the mth row of $\mathbf{H}_k$. In this case, $\gamma_m(\mathbf{H}_k) = ||\mathbf{H}_{k,m}||_F^2$. The MIMO channel capacity is calculated at each OFDM subcarrier using the above equation, while the MIMO-OFDM channel capacity is calculated as an average of the MIMO channel capacity over all OFDM subcarriers at a fixed signal SNR = 20 dB. For our measurement analysis, we chose signal SNR = 20 dB to have an even estimation of the MIMO channel capacity along the path and to emphasize effects of the MIMO channel structure on the capacity. The fixed value of signal SNR = 20 dB was chosen as an example, which is typically used for MIMO channel capacity analysis for the system using 16-quadrature amplitude modulation (QAM) or 64-QAM (e.g., [27, 37])

We note that the MIMO capacity value monotonically increases or decreases with the higher or lower signal SNR and it does not affect the conclusions of comparative analysis of higher or lower MIMO channel capacity as a function of subcarrier spacing or environment as have been performed in this paper. The MIMO channel capacity referred to in this paper corresponds to an

ideal capacity, where it is assumed that a perfect CSI is available at the receiver. The actual capacity is typically reduced from this capacity due to the inaccuracy of the CSI at the receiver, especially in a mobile environment. In addition, the effects of inter-carrier interference (ICI) and inter-symbol interference (ISI) are ignored in this paper. We consider that the effects of ICI are small given the subcarrier spacing used and the maximum Doppler shift assumed. The ISI is expected to be removed by the use of cyclic prefix.

For a SISO fading channel with perfect knowledge of the channel at the receiver, the capacity of a SISO link is given as $C = \log_2(1 + \rho)$. Therefore, the capacity of an equivalent SISO link is equal to approximately 6.66 bps/Hz at ρ.

In this paper, there are two types of SNR being discussed. The first is nominated as ρ in (2) and is referred as signal SNR. The second SNR is referred to as channel estimation (CE) SNR which indicates the quality of the channel estimation.

1.2.3 Maximum LOS MIMO capacity criteria

In conventional MIMO systems, an inter-element antenna spacing equal to $\lambda/2$ is considered to be adequate to avoid strong correlation between received signals [38]. For most indoor applications, this inter-element spacing is still applicable; however, for V2I systems, such spacing cannot be used to achieve maximum capacity due to the larger distance between RX and TX, which tends to reduce the angular spacing and hence to increase correlation between subchannels. Figure 1 shows an example of the geometry of the positions of TX and RX antenna elements and associated parameters in V2I systems. In Fig. 1, θ is the angular spacing between the two MIMO subchannels. We used a 2×2 MIMO system as the basis of our derivation of the maximum capacity criterion. Figure 2 shows a simplified 2D version of the model.

The conditions for achieving the minimum and maximum capacities in a time-invariant or slow time-varying MIMO channel are given below as in [27]. The minimum MIMO capacity is obtained when $\mathbf{H}\mathbf{H}^H = n_t \mathbf{1}_{n_r}$, where $\mathbf{1}_{n_r}$ is an $n_r \times n_r$ all ones matrix. This corresponds to a system with rank-1 $\mathbf{H}_{\text{LOS}}$ response with an associated capacity that is equivalent to that of a SISO channel given as $C_{\min} = \log_2(1 + n_r\rho)$. The capacity in Eq. (2) is maximized for $\mathbf{H}\mathbf{H}^H = n_t \mathbf{I}_{n_r}$, i.e., when $\mathbf{H}$ is orthogonal. This response corresponds to a system with perfectly orthogonal MIMO subchannels, and the capacity of the MIMO channel is then equivalent to that of n_r independent SISO channels given as follows: $C_{\max} = n_r \log_2(1 + \rho)$, $C_{\max}$ corresponds to a maximum capacity value of 13.32 bps/Hz for a 2×2 MIMO system. From the normalized free space channel response matrix of the $n_r \times n_t$ MIMO system given above, the correlation matrix is given as follows:

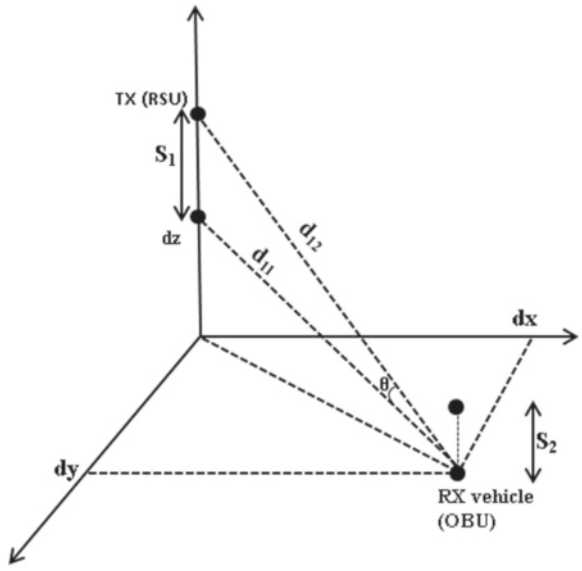

Fig. 1 Positions of TX and RX antenna elements with the RX vehicle (OBU antennas) mounted at the rooftop of a car moving along a street in *x* and *y* directions while the TX roadside unit (RSU antennas) was mounted at a fixed position

$$\mathbf{H}\mathbf{H}^H = \begin{bmatrix} n_t & \cdots & \sum_{m=1}^{n_t} e^{-j\beta(d_{1,m}-d_{n_r,m})} \\ \vdots & \ddots & \vdots \\ \sum_{m=1}^{n_t} e^{-j\beta(d_{n_r,m}-d_{1,m})} & \cdots & n_r \end{bmatrix}$$

In the case of the 2×2 MIMO system, the above equation can be simplified to

$$\mathbf{H}\mathbf{H}^H = \begin{bmatrix} 2 & e^{j\beta(d_{21}-d_{11})} + e^{j\beta(d_{22}-d_{12})} \\ e^{j\beta(d_{11}-d_{21})} + e^{j\beta(d_{12}-d_{22})} & 2 \end{bmatrix}$$

It is clearly seen that the matrices are deterministic and depend on the distance between the TX and RX elements [39]. It can be seen that $\mathbf{H}\mathbf{H}^H$ becomes a square

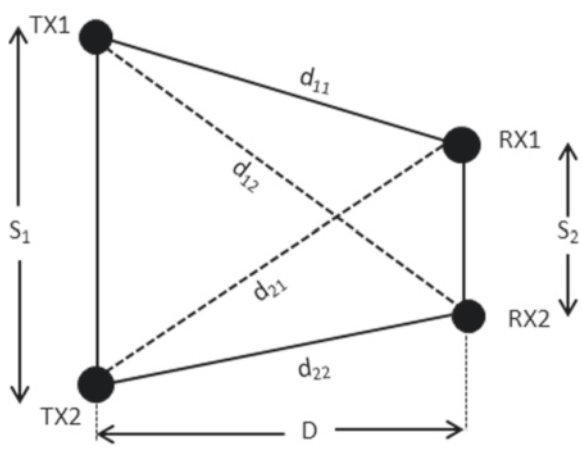

Fig. 2 A 2×2 MIMO near-range LOS system with parallel arrays

matrix in which all the elements of the principal diagonal are twos and all other elements are zeros when $e^{j\beta(d_{11}-d_{21})} + e^{j\beta(d_{12}-d_{22})} = 0$. Based on the mathematical conditions given in the previous paragraph, it is clear that the maximum capacity of a 2×2 MIMO is achieved when

$$\mathbf{H}\mathbf{H}^H = n_t \mathbf{I}_{n_r} = 2\mathbf{I}_2, \tag{4}$$

that is, when all eigenvalues of $\mathbf{H}\mathbf{H}^H$ become equal and we end up with perfectly orthogonal MIMO spatial subchannels. Sarris et al. in [25, 27] have shown that this maximum capacity condition is satisfied when

$$|d_{11} - d_{12} + d_{22} - d_{21}| = (2r+1)\frac{\lambda}{2}, r\epsilon Z^+ \tag{5}$$

where λ is the wavelength at any carrier frequency, Z^+ represents the set of integers, and $(2r+1)$ is an odd integer number. In physical terms, the authors in [25, 27] concluded that Eq. (5) stated that the approximate maximum capacity criterion corresponds to systems where the sum of the path differences $(d_{11} - d_{12})$ and $(d_{22} - d_{21})$ is an odd integer multiple of a half wavelength [27]. In Fig. 3, the RX is moving along the street while the TX is mounted in a fixed position. Both the TX and RX antennas have two antennas on each side.

Equation (5) could be simplified further by making a number of assumptions. First, assume the two antenna arrays are parallel and have inter-element spacings, s_1 and s_2 as illustrated in Fig. 2. Then, $d_{11} = d_{22}$ and $d_{12} = d_{21}$, and hence, the maximum capacity is achieved when

$$|d_{11} - d_{21}| = (2r+1)\frac{\lambda}{4}, r\epsilon Z^+ \tag{6}$$

Figure 1 illustrates a case for a 2×2 MIMO antenna array with a spacing of s_1 at TX and s_2 at RX. The equation for the TX-RX separation distance D and the angle of rotation θ between the first element of each array is defined in [25, 27] as

Fig. 3 TX and RX measurement setup

$$D = \sqrt{dx^2 + dy^2 + dz^2} \tag{7}$$

$$\cos\theta = \frac{\sqrt{dx^2 + dy^2}}{D} \tag{8}$$

For V2I systems, the simplified maximum LOS-MIMO capacity criterion has been given in [13, 14, 25] as

$$s_1 s_2 \approx (r + \frac{1}{2})\frac{D\lambda}{\cos^2\theta}, r\epsilon Z^+ \tag{9}$$

This equation shows that if all s_1, s_2, D, θ, and λ satisfy (9) with a certain $r\epsilon Z^+$, the MIMO capacity will be at its maximum. It is interesting to note that (9) is a function of the inter-element distances (s_1, s_2), the TX-RX separation distance (D), the orientation of the arrays (θ), and the carrier frequency (f_c). Thus, the simplified 2×2 MIMO capacity criterion is expressed in terms of the s_1, s_2, D, θ, and f_c. Equation (5) shows a criterion that should be satisfied to maximize the channel capacity. The criterion is simplified and concluded in (9). This implies that if (9) is met based on the positioning and separation of TX and RX, we will achieve the maximum channel capacity in a 2×2 MIMO system. For a time-invariant channel, λ, D, and θ are constant. As a consequence, the second part of (9) can be constant with a certain $r\epsilon Z^+$. We can satisfy (9) by setting appropriate s_1, s_2, and we can claim that the channel capacity is at its maximum when that is fulfilled. In mobile scenarios, D and θ may vary with the movement of the RX vehicle. To simplify further, the minimum optimal spacing or the first solution of (9) is satisfied when $\theta = 0$ and $r = 0$. Therefore, the antenna separation distance required for optimal LOS MIMO operation is expressed as

$$s_1 s_2 = \frac{D\lambda}{2} = \frac{Dc}{2f} \tag{10}$$

Conceptually, a larger TX-RX separation distance requires larger antenna element spacings, and lower frequencies require larger antenna spacings. For fixed f and D, the antenna arrays could be easily designed so that subchannel orthogonality can be achieved which will result to the attainment of maximum capacity in LOS scenarios. For V2I communications where the RX vehicle is moving, D and θ change with time. Hence, the receiver antenna array is not fixed at a specific position, but its location varies with the motion of the vehicle. The optimal LOS MIMO V2I operation depends on achieving the optimal angle θ_{opt} and separation distance between TX and RX D_{opt}.

1.2.4 Least square channel estimation

The least square channel estimation is needed by many pilot-based channel estimation for MIMO-OFDM as an

initial estimation. It is the simplest approach to pilot-symbol-aided (PSA) channel estimation in OFDM systems, and no a priori information is assumed to be known about the statistics of the channel taps. However, it shows poor accuracy as it is performed on a frame-by-frame basis with no filtering of the estimate. The SISO-OFDM system model at the nth OFDM symbol and kth OFDM subcarrier is given as [29]

$$Y_{n,k} = X_{n,k}H_{n,k} + W_{n,k} \tag{11}$$

$Y_{n,k}$ is the received signals, $X_{n,k}$ is the transmitted signal, and $W_{n,k}$ is the adaptive white Gaussian noise (AWGN). The LS channel estimation $\hat{H}_{\mathrm{LS}^{\mathrm{n,k}}}$ is given as

$$\hat{H}_{\mathrm{LS}^{\mathrm{n,k}}} = \frac{Y_{n,k}}{X_{n,k}} = H_{n,k} + \frac{W_{n,k}}{X_{n,k}} \tag{12}$$

It is important to note that this simple LS estimate $\hat{H}_{\mathrm{LS}}$ does not exploit the correlation of channels across frequency carriers and across OFDM symbols. We utilized the LS estimation approach to get the initial MIMO channel estimates at the pilot subcarriers, which was then further improved using a 2D DCT filtering technique in both time and frequency [30–32]. The effectiveness of this technique is shown in the Section 1.4.

1.3 MIMO-OFDM V2I measurements

1.3.1 Measurement equipment

The 2×2 MIMO-OFDM V2I channel measurements were performed using an in-house built software-defined radio platform using AD9361 dual MIMO RF agile transceivers from Analog Devices, as TX and RX. The AD9361 is a wideband 2×2 MIMO transceiver. It combines an RF front-end with a flexible mixed-signal baseband section with a 12-bit analog-to-digital converter (ADC) and a digital-to-analog converter (DAC) and integrated frequency synthesizers. It provides a configurable digital interface to a processor. It operates from 70 MHz to 6.0 GHz, with tunable bandwidth from 200 kHz to 56 MHz. The equipment transmits channel sounding OFDM signals with three different subcarrier spacings, as shown in Table 1.

A custom-built user interface software running on Windows operating system was used. This software captures ADC samples and records them on a PC's hard disk via USB connection. The transmitter sends OFDM signals to sound the channel, which are eventually recorded at the receiver unit. By post-processing, we then obtained the complex channel transfer function or frequency response as explained in Section 1.2.4. The transmitted OFDM signal waveforms (DAC samples) were generated off-line in the PC, using MATLAB. The in-house built platform is equipped with a field-programmable gate array (FPGA) that streams the off-line generated waveforms to the AD9361's DAC. The baseband-to-RF module amplifies, filters, and up-converts the signals to RF (920 MHz), and the antenna module processes the signals from the RF stage and sends them to the receiver through the MIMO channel. At the receiver side, the signals reach the antennas and pass to the low-noise amplifiers and down converters. The baseband waveform is sampled by the ADC, and the sampled baseband waveform data is transferred to the PC via USB and recorded on the hard disk. Each transmitted OFDM-based wireless packet has an approximate duration of 50 ms. The transmitted OFDM packets were sampled at 32.768 M samples per second. The measurement channel bandwidths are 8.2, 9.0, and 6.7 MHz for LSS, MSS, and SSS, respectively. The transmitted data are modulated by quadrature phase shift keying (QPSK). The OFDM-based wireless packets entirely consisted of the pilot symbols for the purpose of the 2×2 MIMO-OFDM channel measurement.

Table 1 OFDM packet parameters

Parameters	LSS	MSS	SSS
Baseband sample rate (Msps)	32.768	32.768	32.768
Measurement channel bandwidth (MHz)	8.2	9.0	6.7
Center frequency (MHz)	920	920	920
Modulation	QPSK	QPSK	QPSK
No. of OFDM symbols	6003	593	156
No. of occupied subcarriers	52	600	1705
Subcarrier spacing (kHz)	156.25	15	3.348
FFT length	208	2184	8384
OFDM symbol period (μs)	6.4	66.67	299
Guard interval (μs)	1.6	16.67	75

A 2×2 MIMO antenna system was implemented using two commercially available omnidirectional vertically polarized L-COM HGV-906 antennas and two off-the-shelf omnidirectional antennas as both TX and RX antenna array elements, respectively, for all measurements described in this paper. A 35-dBm high-power amplifier ZHL-1000-3W from Mini-Circuits was added at the transmitter to provide an output power of 23 dBm. With the use of a 6-dBi antenna, the maximum effective isotropic radiated power (EIRP) is 29 dBm. The spacing of the antenna elements is set to $\approx 6\lambda$ at TX and $\approx 3\lambda$ at RX where $\lambda = 32.5$ cm, i.e., the spacing between the TX antennas TX1-TX2 $=$ 2 m and between the RX antennas is RX1-RX2 $=$ 1 m. The two transmitter antennas (TX) were mounted at a fixed position each at the same height of $H_{\mathrm{TX}} = 3.6$ m and the two receiver antennas (RX) mounted at the rooftop of a vehicle at a height of $H_{\mathrm{RX}} =$ 1.8 m, as shown in Fig. 3. The measurement platform uses built-in Global Positioning System (GPS) receivers to ensure accurate synchronization of the TX and RX. In

addition, the receiver system was equipped with an external EVK-6T-0 U-blox 6 GPS to provide measurement time stamp as well as the location and speed data for the RX vehicle.

We used a portable Rohde & Schwarz (R&S) FSH8 spectrum analyzer to measure the interference from other devices operating at the 920 MHz band. We observed that the transmitted signal from a nearby cellular base station was causing desensitization of our receiver. As a solution, we used channel filters to remove the effects of the interfering signals during the measurements. No other significant interference in the 920 MHz ISM band was observed during the measurements. All the measurement equipment was separately calibrated with Agilent signal generators and signal analyzers. The TX output power was measured with a power meter. The measurement parameters are summarized in Table 2.

1.3.2 Measurement environments

The MIMO-OFDM V2I measurements were conducted on a suburban street located at CSIRO ICT Centre Laboratory in NSW, Australia. The environment can be characterized as suburban with a two-lane road, some office and residential buildings, cars, parking lots, concrete pillars, metallic sign posts and fences, base station mast, road signs, and high tree density on both sides of the street which provides a rich multipath scattering environment that favors MIMO channels. The measurements took place during working hours at the end of the winter season between 09:00 and 16:00 (GMT+10). The RX vehicle was following a rectangular route as illustrated in Fig. 4. Each measurement scenario was recorded over a duration of 10 min for five different rounds. The capturing of the ADC samples was not performed continuously, and as such, the acquired data was limited to 5 GB. The maximum separation distance and relative speed between the TX and RX antenna were derived from the GPS location, and speed data was 250 m and 55 km/h, respectively. The separation distance varied between 3 and 250 m. Occasional blockage of the LOS occurred due to high tree density and buildings. Both LOS and NLOS conditions existed during the measurements. Significant scatterers in the surrounding environment are trees, buildings, residential houses and offices, traffic signs, metallic fences, and moving and parked cars that can significantly contribute to a multipath propagation environment. In the measurement scenarios, we transmitted OFDM packets with the parameters shown in Table 1. The minimum guard interval of 1.6 μs was considered to be large enough to remove ISI in this short-range outdoor environment.

Table 2 Measurement parameters

Parameters	Values
MIMO system	2 × 2
Center frequency	920 MHz
Packet duration	50 ms
Sampling frequency	32.768 Msps
Transmit power	23 dBm
TX antenna gain	6 dBi
RX antenna gain	2 dBi
TX antenna spacing	2 m
RX antenna spacing	1 m
TX antenna height, h_{TX}	3.6 m
RX antenna height, h_{RX}	1.8 m
Modulation	QPSK

1.4 Measurement results and analysis

The post-processing of measurement data was performed using MATLAB. The measured MIMO channels are estimated from the received signals. In particular, the channel coefficients were estimated by LS channel estimation by sending known channel training symbols alternately in time using the two transmitters (e.g., the first transmitter sent channel training symbols at odd OFDM symbol time index and the second transmitter sent channel training symbols at even OFDM symbol time index). The transmitted wireless packets have a duration of 50 ms and consist of all known channel training symbols.

The measurement system was equipped with GPS receivers at both the TX and the RX ends for accurate time reference (less than 100 ns ambiguity), which facilitated frame detection and time offset estimation. The GPS receivers also provided accurate frequency reference which removed the necessity of frequency offset estimation and correction. Residual frequency offset which was less than 100 Hz was included in the estimated channel. No additional ICI cancelation technique was applied, apart from the fact that the TX and the RX frequency references were synchronized to the GPS reference, which we expect to reduce the ICI problem significantly. We note that the Doppler shift expected in the measurement at 920 MHz with up to 55 km/h is approximately 47 Hz. Given the minimum subcarrier spacing of approximately 4 kHz (corresponding to SSS), we consider that the effects are negligible.

We used a high sampling rate of 32.768 Msps for the measurement to reduce the effect of noise. The use of oversampling to improve the SNR in OFDM transmission has been proposed in the literature [40, 41]. Random receiver noise is reduced by oversampling based on the assumption that the signal is coherent and that the noise is random. We extended our analysis to remove the effects of channel estimation errors by applying 2D DCT filtering in both time and frequency [30–32]. The 2D DCT has significantly reduced the effect of noise on our measurement

Fig. 4 Google Earth map view of the measured location data from the GPS showing the location of the TX and RX route round the measurement environment. The *blue line* shows the route taken by RX, and and *yellow dot* shows the fixed location of TX. The indicated driving route outside roads are considered to be due to errors in estimating locations

results. In addition, we have included a simulation analysis to show that the effects of channel estimation error on MIMO channel capacity are small for high SNR up to 20 dB.

1.4.1 Effects of channel estimation error on MIMO channel capacity

We investigated the effects of channel estimation error on the MIMO capacity for i.i.d. Rayleigh fading channels by simulation. Figure 5 presents the deviation of the estimated capacity with channel estimation error for three different CE SNR (10, 20, and 30 dB) in the case of 2×2 MIMO. Figure 5 clearly shows that a significant deviation in the measured MIMO channel capacity may result where the CE SNR is 10 dB, while the 30 dB CE SNR gives insignificant deviation.

We applied 2D DCT-based filtering to reduce the effects of the channel estimation error and noise on our measurement results. Figures 6 and 7 present the measured 2×2 MIMO-OFDM doubly selective channel frequency response for the non-noise-reduced and noise-reduced MSS, respectively. The presented results correspond to NLOS propagation conditions. These are samples of the

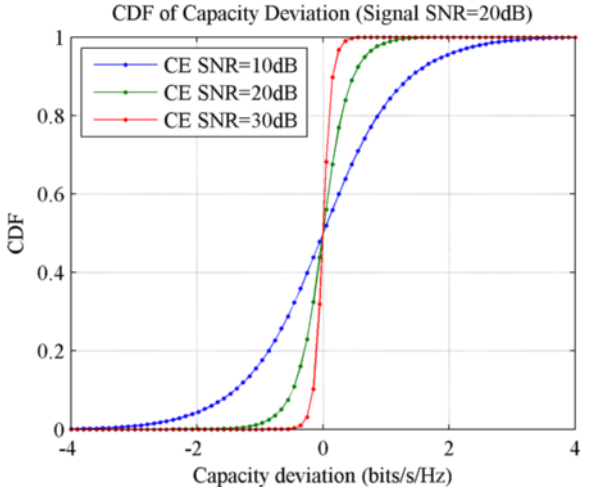

Fig. 5 CDF of capacity deviation at signal SNR = 20 dB for different channel estimations

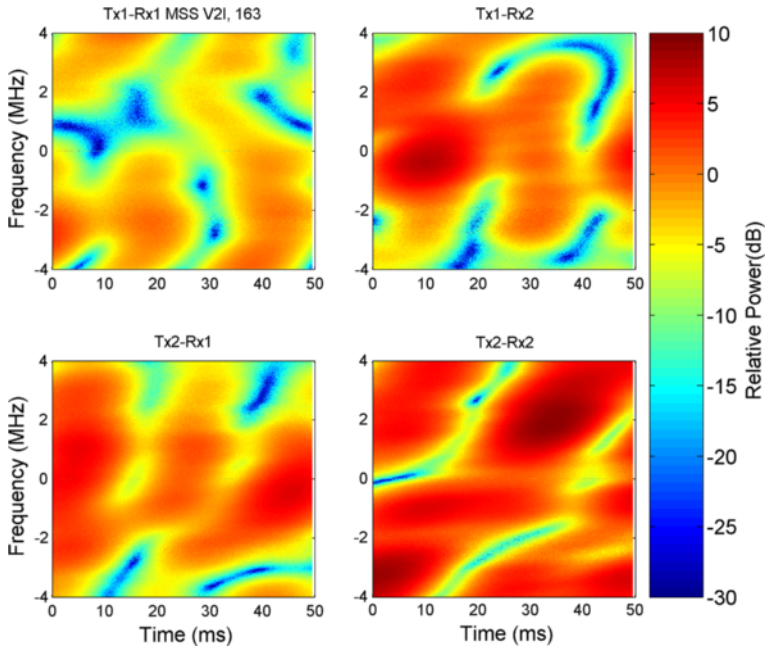

Fig. 6 Example of measured 2 × 2 MIMO-OFDM non-noise-reduced doubly selective channel for the MSS case

MIMO subchannels considered at a time when the RX vehicle is in motion at receiver position, $d = 200$ m. Variations in frequency and in time are evident from the results. Figures 6 and 7 show that the effects of channel estimation error on the measured MIMO channel have been reasonably reduced by employing 2D DCT filtering in both time and frequency. Figure 8 shows an example time variation of the MIMO subchannel at one OFDM subcarrier in a LOS environment with the MSS case. The blue dots show the original LS-estimated channel while the red curve shows the 2D DCT filtered version. Figure 9 shows an example for a NLOS case. It can be seen that

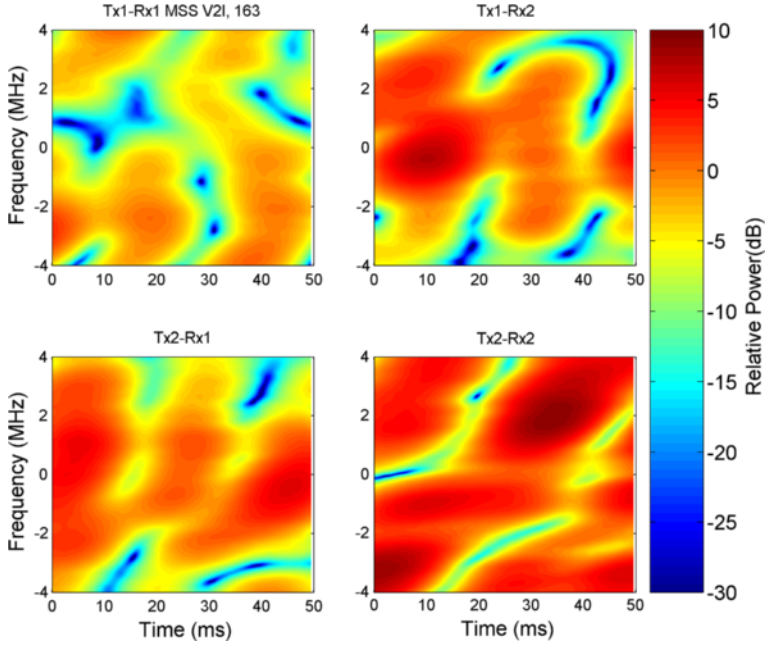

Fig. 7 Example of measured 2 × 2 MIMO-OFDM 2D DCT noise-reduced doubly selective channel in NLOS for the MSS case

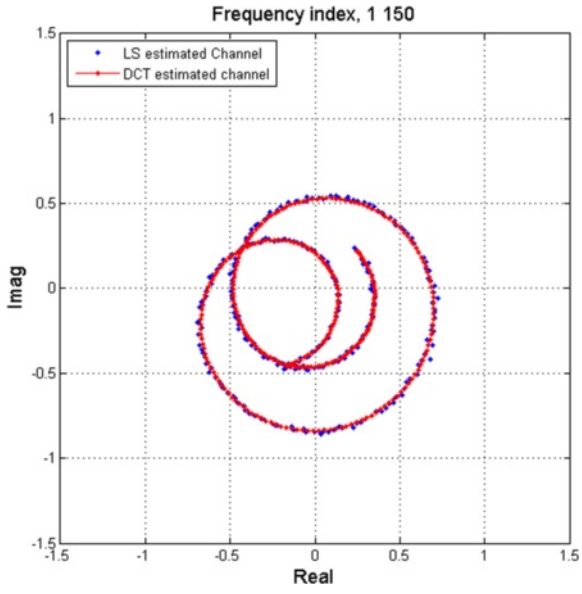

Fig. 8 Time variation of MIMO channel at one frequency for 2D DCT noise-reduced estimated channel and the LS-estimated channel at LOS $D = 34.3$ m

the LS-estimated MIMO channel follows the 2D DCT noise-reduced MIMO channel.

We approximately estimated the measured CE SNR as the difference between the noise-reduced MIMO channel and the LS-estimated MIMO channel, assuming that the noise-reduced MIMO channel is ideal. The results are averaged over time and frequency. The same method was used for the three different subcarrier spacing scenarios. Figure 10 presents the measured CE SNR as a function of the receiver position for the three different subcarrier spacings considered. The figure shows that the CE SNR indeed varies as a function of the receiver position and the separation distance. It shows the mean CE SNR for all locations having at least 15 dB. The measured CE SNR information as shown in Fig. 10 has practical value in understanding what distance can be achieved with a practical transmitting power value. However, we consider that it is important to separate the effects of CE SNR and the effects of the physical environment in analyzing the MIMO channel capacity. For this reason, we have chosen to use what we call fixed signal SNR criteria (transmitting power can be unlimitedly adjusted to provide fixed signal SNR at all receiver locations within the coverage) in analyzing the MIMO channel capacity in this paper. An example value of signal SNR = 20 dB was chosen for our MIMO capacity analysis, as this is typical for a wireless communication using 16-QAM or 64-QAM depending on the forward correction coding rate. In our actual measurement, automatic gain control (AGC) was used to adjust the gain at the receiver but not to the extent to assure the CE SNR of 20 dB at all measurement location, causing the channel estimation error corresponding to the CE SNR.

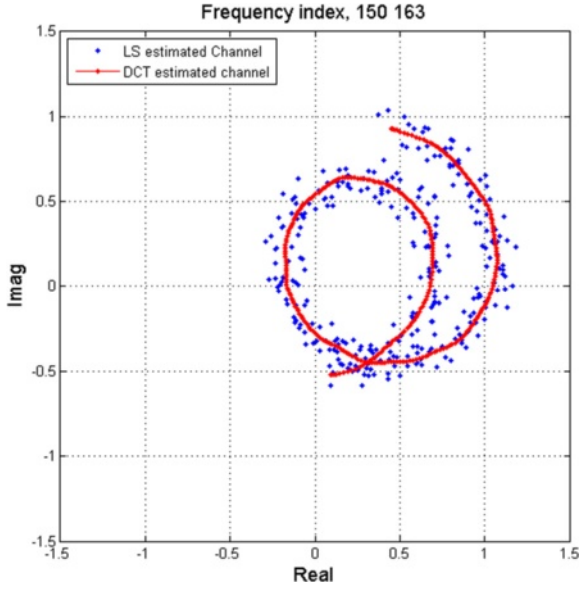

Fig. 9 Time variation of MIMO channel at one frequency for 2D DCT noise-reduced estimated channel and the LS-estimated channel at NLOS $D = 200$ m

1.4.2 *Measured MIMO-OFDM channel capacity variation as a function of the measurement time*

From the collected data, the MIMO channel capacity was calculated based on Eq. (2) for the three different subcarrier spacing values considered. It is well known that MIMO channels depend on the values of the channel response matrix, the number of TX and RX antenna

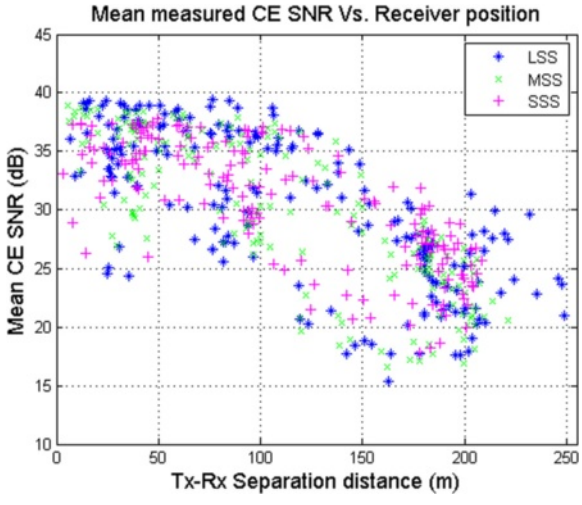

Fig. 10 Example of mean measured channel estimation SNR as a function of TX-RX separation distance (m)

arrays, and the signal SNR at the receiver. The capacity evaluated at a fixed signal SNR is a measure of scattering richness of a MIMO channel and allows the analysis of capacity degradation due to the influence of spatial correlation when changing from LOS to NLOS conditions. The TX and RX antenna arrays are both individually separated at distances of approximately 6λ and 3λ, respectively, to reduce the influence of correlation. Figure 11 shows significant variations in mean capacity for different measurement times, ranging from a maximum of 13.6 bps/Hz to a minimum of 8.4 bps/Hz for all subcarrier spacing scenarios considered.

1.4.3 Cumulative distribution function of MIMO capacity

Table 3 presents the cumulative distribution function (CDF) of the MIMO channel capacity for the three different subcarrier spacings considered: LSS, MSS, and SSS. Figure 12 presents the measured CDF of MIMO-OFDM channel capacity. Our analysis reveals that there is no significant variation in the MIMO capacity for the different OFDM standard subcarrier spacings considered for LSS, MSS, and SSS scenarios. This implies that any subcarrier spacing could be used in MIMO-OFDM systems to achieve optimal performance in terms of capacity. The dynamic range is defined in [3] as the difference between the maximum and the minimum values of the MIMO channel capacity. In this paper, we consider the 90 % capacity dynamic range $C_{\mathrm{DR}(90\,\%)}$ as the difference between the 95 % ($C_{95\,\%}$) and 5 % ($C_{5\,\%}$) mean capacity values evaluated from the CDF of mean MIMO capacity. The measured $C_{\mathrm{DR}(90\,\%)}$ are 3.3, 3.6, and 4.4 bps/Hz, respectively, for LSS, MSS, and SSS scenarios. Table 3 summarizes the dynamic range of mean MIMO-OFDM capacity for the three different subcarrier spacing scenarios considered. The CDF plots show there is a 10 % probability of the mean 2 × 2 MIMO channel capacity being below 9.7 bps/Hz and a 50 % probability of the mean capacity being below (or above) 11.4 bps/Hz for all the three scenarios considered. Furthermore, there is a 90 % probability of the mean capacity being below 12.2 bps/Hz for LSS cases, 12.5 bps/Hz for MSS cases, and 13.1 bps/Hz for SSS cases. In conclusion, lower capacity values in the range of 8 to 11 bps/Hz are achieved equally by all the subcarrier standards studied. However, higher capacity values on the order of 13 to 14 bps/Hz are achieved by the shorter subcarrier spacing standard (SSS) with higher probability. Currently, we do not have any theoretical reason for the variation of mean MIMO capacity values for different OFDM subcarrier spacings, and we encourage further investigation by researchers.

Table 3 Comparison of the CDF of MIMO capacity for all the three subcarrier spacing scenarios, *C* (in bps/Hz)

Standards	$C_{5\,\%}$	$C_{10\,\%}$	$C_{50\,\%}$	$C_{90\,\%}$	$C_{95\,\%}$	$C_{\mathrm{DR}(90\,\%)}$
LSS	9.2	9.7	11.4	12.2	12.4	3.2
MSS	9.2	9.7	11.4	12.5	12.8	3.6
SSS	9.2	9.7	11.4	13.0	13.5	4.3

1.4.4 MIMO capacity as a function of time and frequency

Figures 13, 14, 15, 16, 17 and 18 show the MIMO channel capacity as a function of time and frequency for LSS, MSS, and SSS cases, each with LOS and NLOS scenarios. For the LSS case, it can be seen that channel capacity *C* varies from 7.8 to 15.0 bps/Hz for the LOS scenario in Fig. 13. Larger variations within 50 ms can be observed (from 6.0 to 15.2 bps/Hz) when the vehicle is moving at higher speed and is under NLOS conditions, as shown in

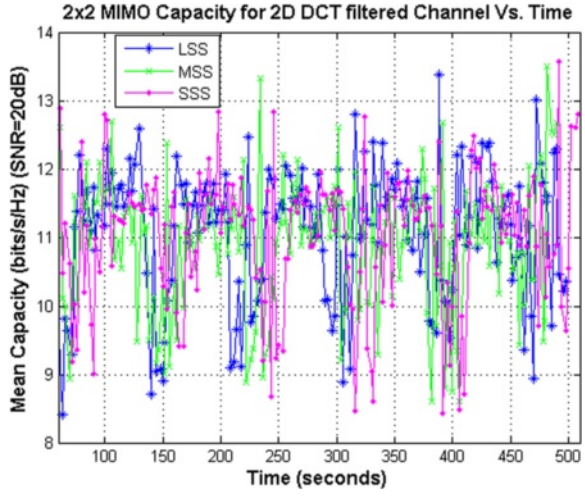

Fig. 11 2 × 2 measured MIMO-V2I channel capacity variation as a function of the measurement time

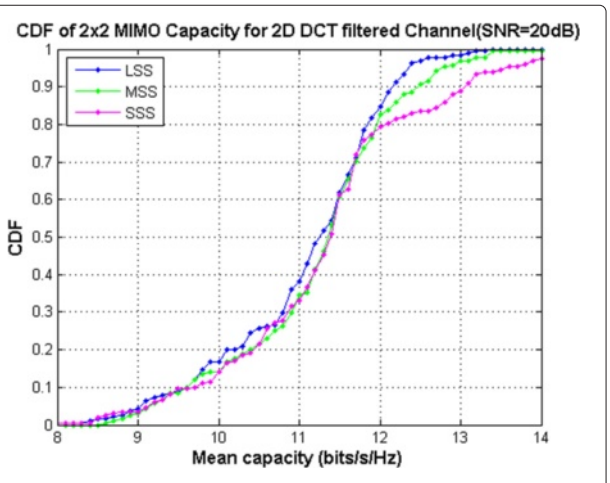

Fig. 12 CDF of MIMO-OFDM channel capacity for three different subcarrier spacings: LSS, MSS, and SSS channel at signal SNR = 20 dB

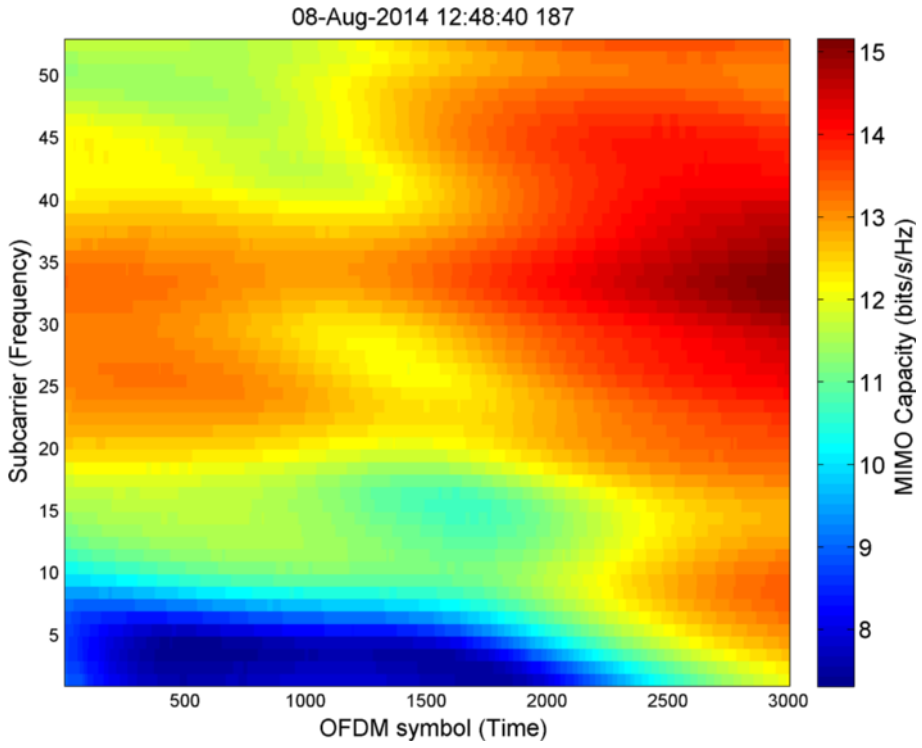

Fig. 13 Example of the measured 2 × 2 LOS MIMO-OFDM V2I channel capacity at $D = 29.8$ m for the LSS scenario

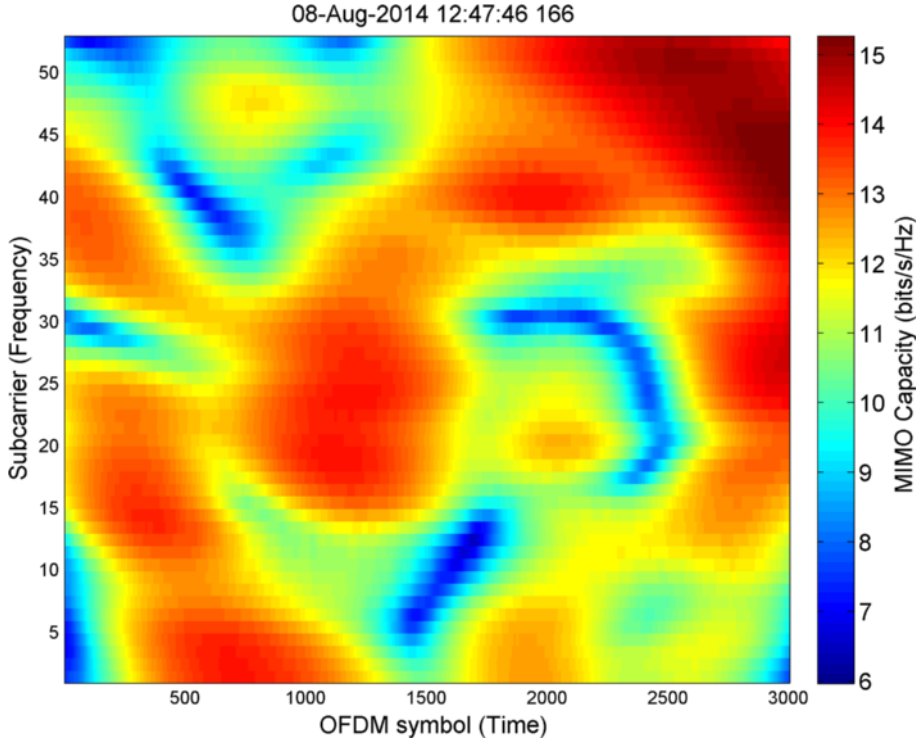

Fig. 14 Example of a measured 2 × 2 NLOS MIMO-OFDM V2I channel capacity at $D = 213.8$ m for the LSS scenario

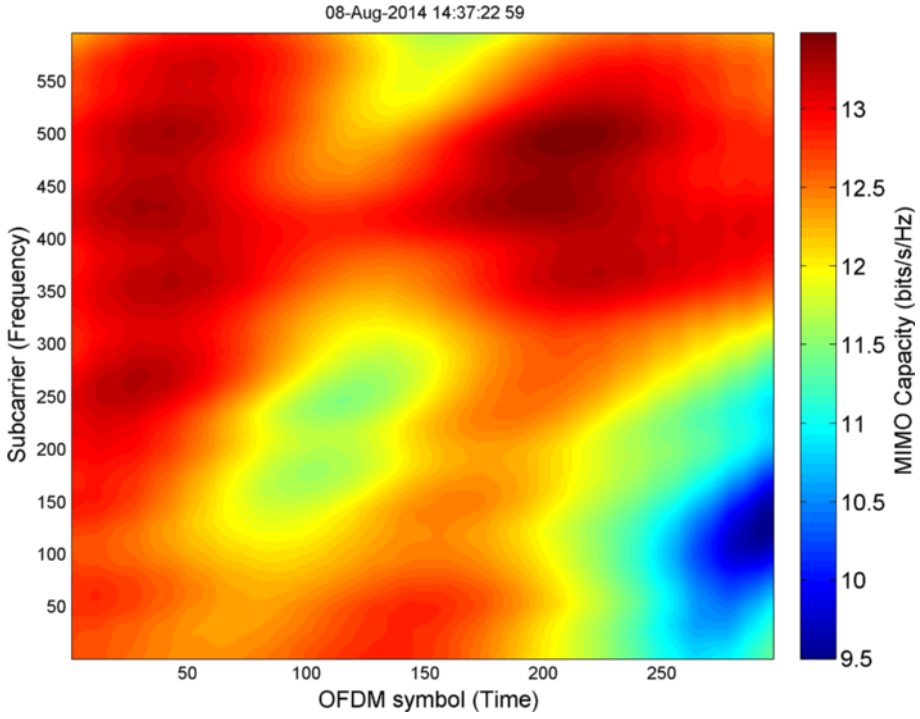

Fig. 15 Example of a measured 2 × 2 LOS MIMO-OFDM V2I channel capacity at $D = 19.98$ m for the MSS scenario

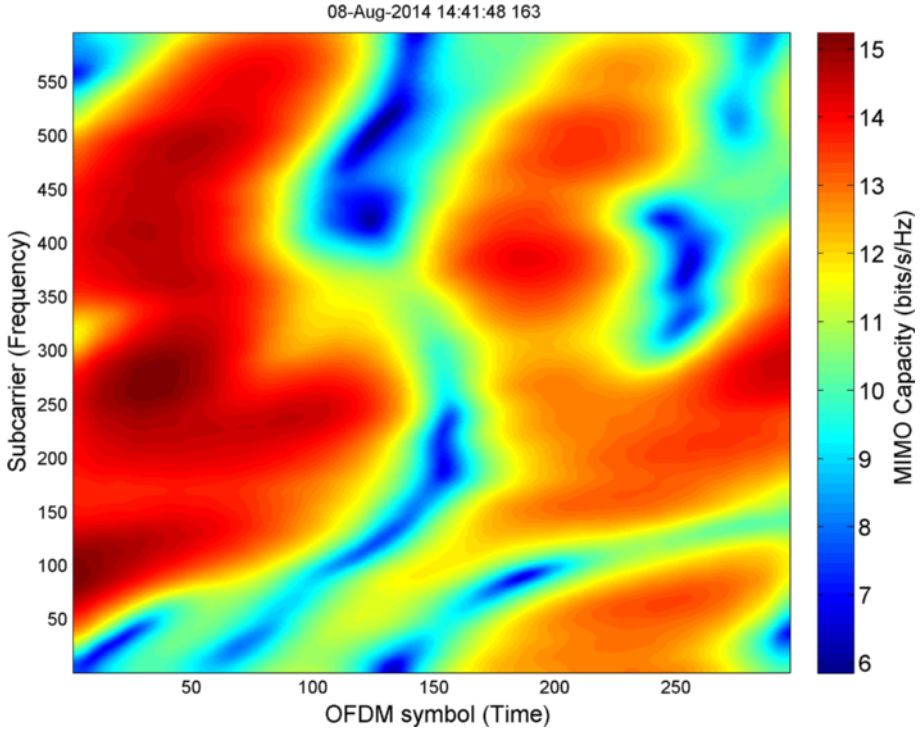

Fig. 16 Example of a measured 2 × 2 NLOS MIMO-OFDM V2I channel capacity at $D = 200$ m when the RX vehicle is moving for the MSS scenario

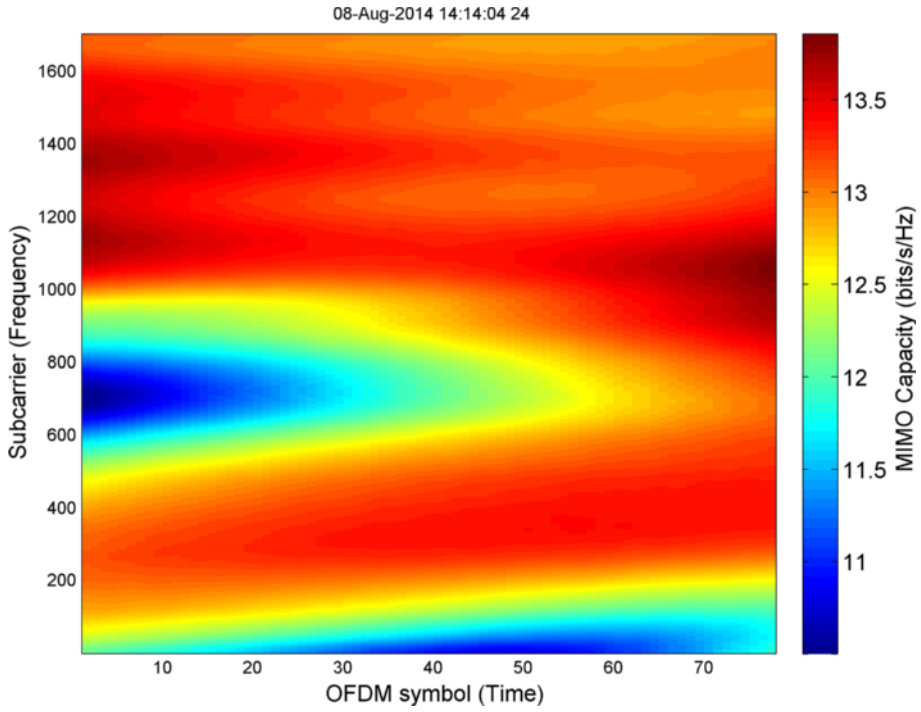

Fig. 17 Example of a measured LOS 2 × 2 MIMO-OFDM V2I channel capacity at $D = 40$ m for the SSS scenario

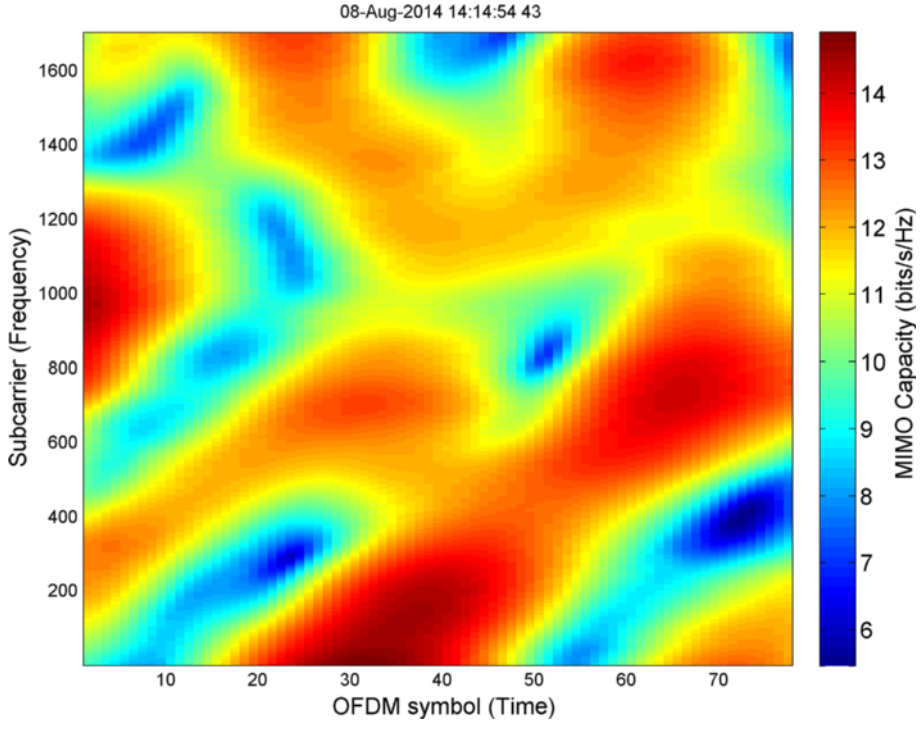

Fig. 18 Example of a measured NLOS 2 × 2 MIMO-OFDM V2I channel capacity at $D = 206$ m when the RX vehicle is moving for the SSS scenario

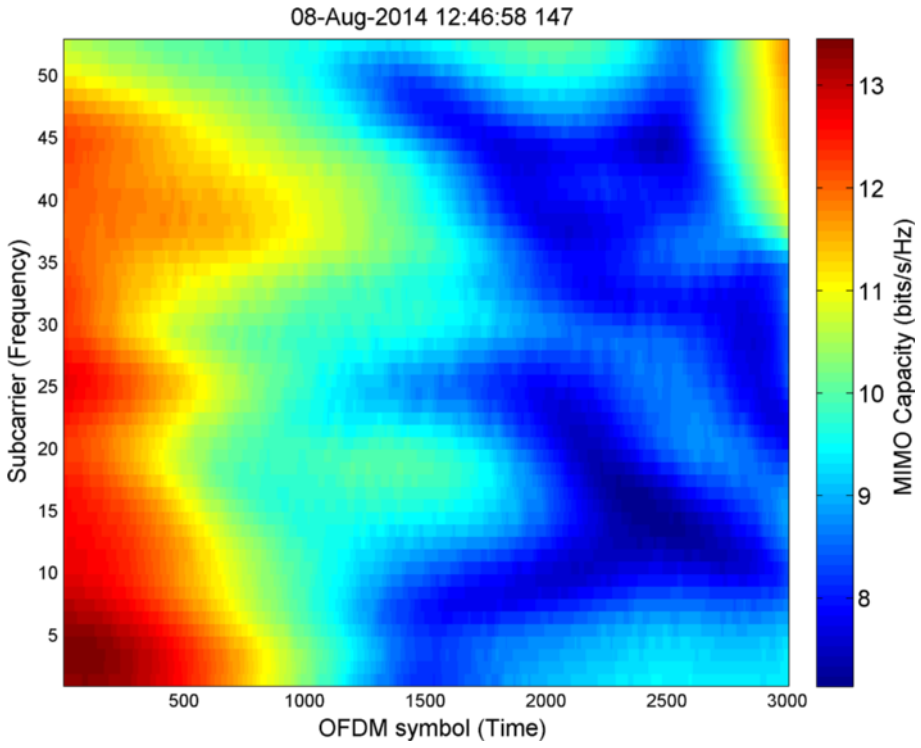

Fig. 19 Example of a measured LOS 2 × 2 MIMO-OFDM V2I maximum channel capacity, $C_{max} = 13.37$ bps/Hz, $D = 76.7$ m for the LSS scenario

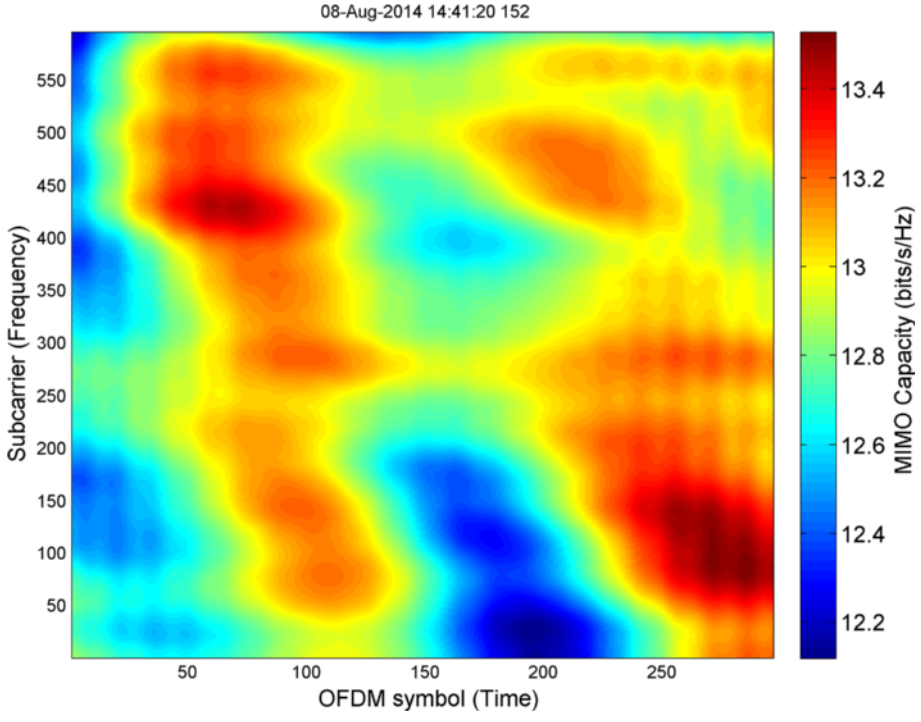

Fig. 20 Example of a measured LOS 2 × 2 MIMO-OFDM V2I maximum channel capacity, $C_{max} \approx 13.0$ bps/Hz, $D = 13.1$ m for the MSS scenario

Fig. 14. For the MSS case, the capacity varies from 9.5 to 13.5 bps/Hz for LOS in Fig. 15 and from 6.0 to 15 bps/Hz for NLOS scenario in Fig. 16. And for the SSS case, the capacity varies from 10.5 to 14.0 bps/Hz and from 5.5 to 15.0 bps/Hz for LOS and NLOS scenarios, respectively. Generally, greater channel capacity dynamic range could be observed for NLOS conditions that involve larger TX-RX separation distances compared to the near-range LOS scenarios.

Figures 19, 20, and 21 present the measured maximum MIMO channel capacity for the LSS, MSS, and SSS scenarios, respectively. Interestingly, the maximum capacity $C_{\max}$ for each scenario was achieved when there was a LOS path between RX and TX. Generally, it can be seen that for some subcarriers, the capacity is high, up to $C_{\max} = 15.0$ bps/Hz (resulting in better performance in terms of data rate link), while for other subcarriers, it is low, at $C_{\min} = 4.0$ bps/Hz (resulting in lower data rate link). These results show that the MIMO capacity significantly varies with different subcarrier indexes and OFDM symbols. In this measurement, the number of scatterers increases when the TX-RX separation distance increases, leading to the de-correlation of the MIMO subchannels and therefore an increase in capacity. When the TX-RX separation distance is small and a strong LOS component exists, the MIMO channel capacity is still large due to the larger angular spacing between the different MIMO subchannels which occur at small TX-RX separation distances. This large angular spacing between the different MIMO propagation paths causes orthogonality, which in turn increases the LOS MIMO channel capacity.

1.4.5 MIMO channel capacity against separation distance

Figure 22 presents the (mean) MIMO-OFDM channel capacity averaged over 50 ms packet time as a function of separation distance between TX and RX. For the LSS case, the maximum MIMO channel capacity is 13.37 bps/Hz, followed by 13.17 bps/Hz at separation distances of 76.7 and 15 m and at a relative speeds of 31.7 and 8.8 km/h, respectively. For the MSS case, the maximum mean MIMO capacity is ≈13.0 bps/Hz, followed by 13.0 bps/Hz at separation distances of 13.1 and 29.6 m and at the relative speeds of 29.3 and 15 km/h, respectively. While for the SSS case, the maximum mean MIMO capacity is 13.57 bps/Hz, followed by 12.8 bps/Hz at separation distances of 62 and 18.4 m and at the relative speeds of 21.6 and 28.3 km/h, respectively. The reason for the measured maximum mean MIMO-OFDM capacity being higher than the theoretical maximum 2×2 MIMO capacity of 13.32 bps/Hz is considered to be due to the averaging over the OFDM subcarriers.

From the observation of the environment, we approximately categorized the scenarios as follows. The TX-RX separation distances of less than 100 m were categorized

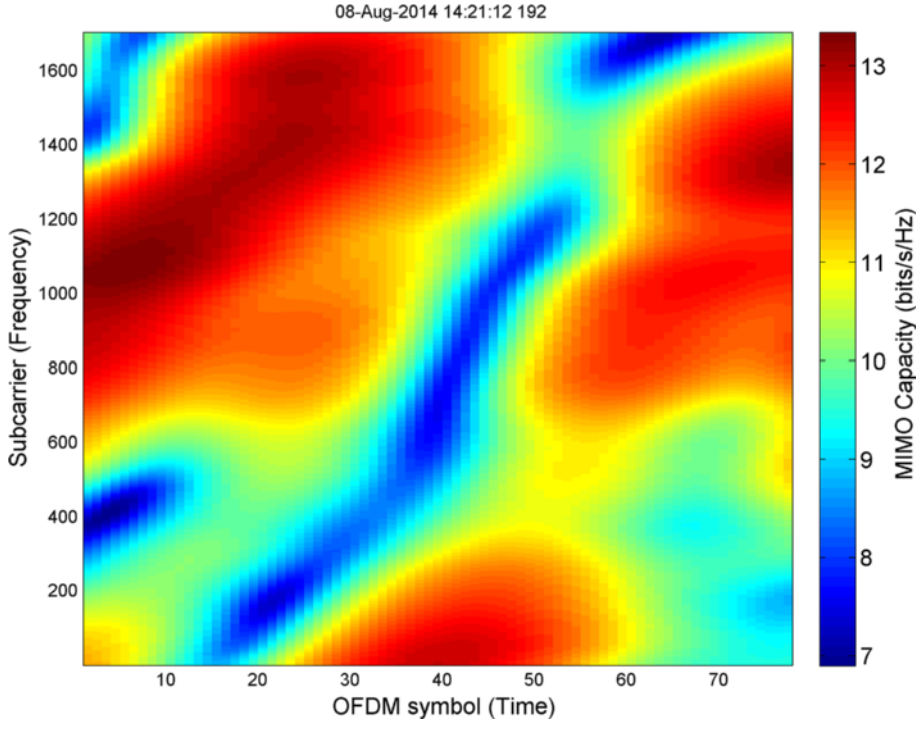

Fig. 21 Example of a measured LOS 2×2 MIMO-OFDM V2I maximum channel capacity, $C_{\max} = 13.57$ bps/Hz, $D = 59$ m for the SSS scenario

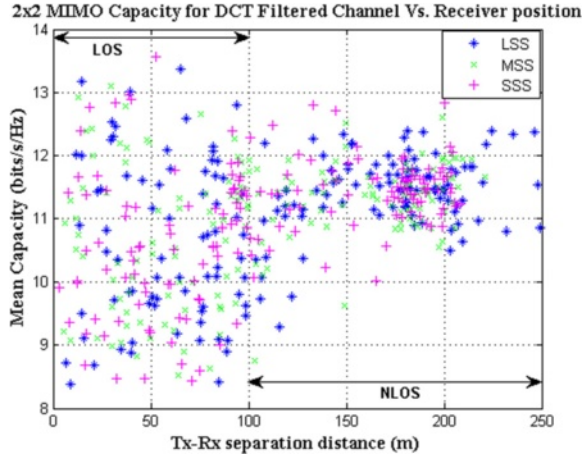

Fig. 22 2 × 2 MIMO capacity for 2D DCT filtered MIMO channel as a function of TX-RX separation distance

as the LOS path. The TX-RX separation distances of more than 100 m were categorized as NLOS scenario. These assumptions match with the geometry of the measurement environment. It is evident that there is an increase in the local minima of the mean capacity, as the separation distance between TX and RX links increases for all the three subcarrier spacings. This is possible due to the expected lower spatial correlation between the different MIMO subchannels caused by the presence of NLOS and a larger number of scatterers (trees, vegetation, metallic fence, buildings, and sometimes moving vehicles) as TX and RX separation distance increases. The lower capacity values in LOS may be due to the degenerated channels typical in the LOS case, while the higher capacity values in LOS compared to NLOS can be explained by the greater angular spacing of the MIMO subchannels. Figures 23 and 24 present the histogram and CDF representations of the mean capacity results for the LOS (in blue curve) and the NLOS (in red curve) MSS scenarios, respectively. The histogram and CDF figures clearly show that the highest mean capacity are achieved for the LOS and also the variance of the mean capacity is much higher for the LOS than for the NLOS scenario. Similar results were obtained for the other two subcarrier spacings.

In general, Fig. 22 clearly shows a correlation between the MIMO channel capacity variation and the TX-RX separation distance, i.e., MIMO channel capacity has a larger variation in near-range LOS conditions and a smaller capacity variation in far-range NLOS conditions. The possible cause of the larger capacity variations for near-range LOS propagation is greater angular spacing between the MIMO subchannels. There is greater angular spacing between the MIMO subchannels for LOS links and less angular spacing between the MIMO subchannels for far-range NLOS links, as illustrated in Fig. 2. Figure 2 shows that as the degree of angular spacing between the MIMO subchannels becomes smaller, the correlation between the received signals becomes larger, as the differences in the length of the MIMO subchannel paths decrease. This greater angular spacing causes the different MIMO propagation paths d_{11} and d_{12}, as well as d_{21} and d_{22}, to be orthogonal, therefore increasing the expected channel capacity. The figure explains our rationale to relate the degree of angular spacing between the MIMO subchannels and the correlation between the received signals. Most LOS conditions in our measurements met the criteria for maximum capacity as stated in Eq. (6), which indicates that the propagation paths should meet the conditions d_{11} and d_{12} and d_{21} and d_{22} that occur when both the TX and RX arrays are parallel. These conditions are

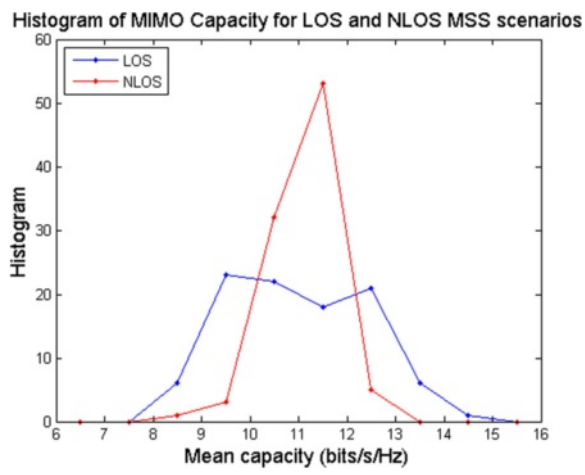

Fig. 23 Histogram of 2 × 2 MIMO channel capacity for LOS and NLOS MSS scenarios

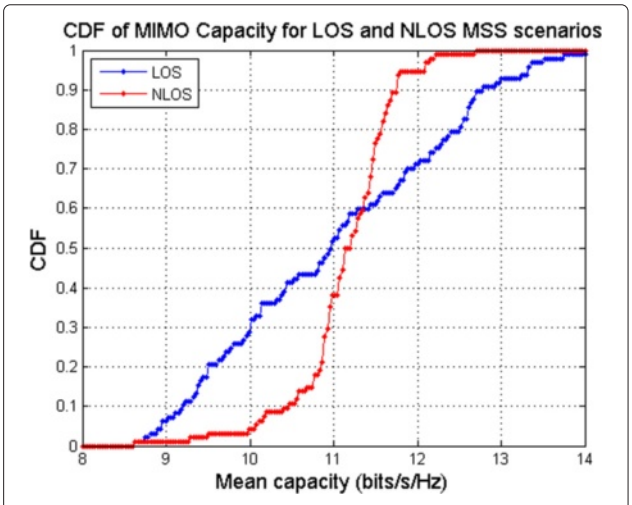

Fig. 24 CDF of 2 × 2 MIMO channel capacity for LOS and NLOS MSS scenarios

met in most of the measured LOS scenarios discussed in this paper. The results presented in this section are consistent with what is expected, as they show that the mean MIMO capacity varies according to the degree of angular spacing between the MIMO subchannels and the correlation between the received signals.

It is observed that the maximum capacities for all subcarrier spacing scenarios were achieved by the LOS case despite the assumed highly correlated channel. This is a surprising result, because signal SNR is not a function of location in our analysis since we considered a fixed signal SNR = 20 dB in order to separate the effects of signal SNR variations. In this measurement, TX-RX antenna arrays are separated far apart on each side of the link (TX = 6λ and RX = 3λ) which is considered to contribute to the de-correlation of the MIMO subchannels in near-range LOS scenarios and to result in a full-rank MIMO channel and lead to the achievement of maximum MIMO capacity in LOS scenarios. The results are consistent with the phenomenon known as LOS MIMO in the literature [14, 24, 25, 42].

Based on the maximum LOS MIMO capacity criteria presented in the previous sections, we investigated a 2×2 MIMO V2I system operating in LOS and NLOS conditions. The TX-RX separation distance D varies between 3 and 250 m as the RX vehicle drives away from TX at a carrier frequency $f = 920$ MHz and fixed antenna array spacing $s_1 = 2$ m at TX and $s_2 = 1$ m at RX; θ and D_{opt} varies as the RX vehicle drives around the vicinity. At a TX height of 3.6 m and a RX height of 1.8 m, the calculated optimal LOS TX-RX separation distance D_{opt} that will satisfy (9) for $r = 0$ and $\theta = 40^\circ$ is $D_{\text{opt}} = 7.8$ m.

In our MIMO-OFDM MSS case, the measured $C_{\max} \approx 13.0$ bps/Hz which is the same as the theoretical maximum LOS-MIMO capacity $C_{\max} = 13.0$ bps/Hz that was achieved at a LOS path corresponding to the theoretical $D_{\text{opt}} = 13.1$ m, which satisfies (9) for fixed $f = 920$ MHz, $s_1 = 2$ m, $s_2 = 1$ m, $\theta = 0$, and $r = 0$. While for the case of LSS and SSS, a higher value than the theoretical maximum capacity of $C_{\max} = 13.37$ bps/Hz and $C_{\max} = 13.57$ bps/Hz, respectively, was achieved at LOS distances of $D = 76.7$ m and $D = 62$ m, respectively. This shows that our antenna spacing satisfied the criterion for achieving the maximum MIMO capacity in LOS situations by proper positioning or spacing of the antenna elements in such a way to achieve orthogonality between spatially multiplexed signals of MIMO systems, resulting in a high-rank channel response matrix. In conclusion, all the maximum capacity values were achieved at near-range LOS and the measured capacity shows very close agreement with the theoretical values of optimal LOS MIMO capacity with very small variations which we attribute to minor inaccuracies in the positioning and orientation of the antenna elements. This validates the LOS maximum capacity criterion for achieving orthogonality between spatially multiplexed signals of MIMO systems in LOS channels by employing specifically designed antenna arrays.

2 Conclusions

A novel 2×2 MIMO testbed has been designed and implemented for three different subcarrier spacings. The MIMO testbed is based on a software-defined radio platform where flexible signal processing can be implemented. The testbed has been used to carry out measurements at a frequency of 920 MHz. We have investigated the channel capacity of a MIMO-OFDM V2I channel under both LOS and NLOS propagation scenarios. We examined a method to achieve orthogonality between spatially multiplexed signals in MIMO V2I communication systems operating in a LOS channel. Our analytical results show that the maximum capacity can be achieved under LOS scenario with proper antenna element spacing despite the effects of higher correlation and reduced rank of the channel response matrix which can be counterbalanced by deliberate separation of antenna elements that preserves orthogonality; this results in a full-rank MIMO channel matrix, and thus, high MIMO capacity is achieved in LOS cases. As anticipated, when the vehicle is driving closer to the TX roadside infrastructure unit, the greatest capacity values are observed in LOS conditions. We observed that even with some deviation from optimal design, the LOS MIMO case outperforms the theoretical i.i.d. Rayleigh performance (11.5 bps/Hz) in terms of Shannon capacity. We investigated the MIMO channel capacity for different positions of the receiver vehicle. Interestingly, since the maximum capacity of LOS-MIMO systems does not depend on the existence of scatterers, there is no particular limit on the linear increase of the system capacity. The presented results demonstrate that the MIMO channel benefits from the movement of the receiver from NLOS to LOS conditions, as the detrimental effect of increased correlation between the received signal is outweighed by the advantageous effect of high angular spacing of the sub-paths. These results show the strong dependence of the MIMO capacity on antenna array spacing and the correlation of the channel response matrix. This measurement demonstrates the significance of using optimally interspaced MIMO antenna array elements at each of the radio links to increase the capacity of MIMO systems over SISO systems.

Competing interests
The authors declare that they have no competing interests.

Acknowledgements
The authors would like to thank the QUT High Performance Computing (HPC) and the Research Support services for their technical assistance during the data analysis. The authors thank Alex Grancea and Joseph Pathikulangara from CSIRO ICT Centre NSW, Australia, for the development of the SDR platform used for the measurements.

Author details
[1]School of Electrical Engineering and Computer Science, Queensland University of Technology, Brisbane, QLD 4001, Australia. [2]CSIRO ICT Centre, Epping, NSW 1710, Australia.

Received: 1 December 2014 Accepted: 14 May 2015
Published online: 25 June 2015

References

1. G Foschini, M Gans, On limits of wireless communications in a fading environment when using multiple antennas. Wirel. Pers. Commun. **10**(6), 311–335 (1998)
2. H Cheng, H Shan, W Zhuang, Infotainment and road safety service support in vehicular networking. Elsevier J. Mech. Syst. Signal Process. **2010**, 1–19 (2010)
3. W K Ziri-Castro, N Scanlon, Evans, Prediction of variation in MIMO channel capacity for the populated indoor environment using a radar cross-section-based pedestrian model. IEEE Trans. Wirel. Commun. **4**(3), 1186–1194 (2005)
4. H Suzuki, T Van, I Collings, Characteristics of MIMO-OFDM channels in indoor environments. EURASIP J. Wirel. Commun. Netw. **2007**(19728), 1–9 (2007)
5. A Goldsmith, S Jafar, N Jindal, S Vishwanath, Capacity limits of MIMO channels. IEEE J. Sel. Areas Commun. **21**(5), 684–702 (2003)
6. A Molisch, M Steinbauer, M Toeltsch, E Bonek, R Thoma, Capacity of MIMO systems based on measured wireless channels. IEEE J. Sel. Areas Commun. **20**(3), 561–569 (2002)
7. GXu Y Yang, H Ling, An experimental investigation of wideband MIMO channel characteristics based on outdoor non-LOS measurements at 1.8 GHz. IEEE Trans. Antennas Propag. **54**(11), 3274–3284 (2006)
8. J Karedal, F Tufvesson, N Czink, A Paier, C Dumard, T Zemen, C Mecklenbrauker, A Molisch, A geometry-based stochastic MIMO model for vehicle-to-vehicle communications. IEEE Trans. Wirel. Commun. **8**(7), 3646–3657 (2009)
9. J Ling, D Chizhik, D Samardzija, R Valenzuela, Peer-to-peer MIMO radio channel measurements in a rural area. **6**(9), 3229–3237 (2007)
10. J Karedal, F Tufvesson, N Czink, A Paier, C Dumard, T Zemen, C Mecklenbrauker, A Molisch, in *Communications, 2009. ICC '09. IEEE International Conference on*. Measurement-based modeling of vehicle-to-vehicle MIMO channels (Dresden, 14–18 June 2009), pp. 1–6
11. O Renaudin, V Kolmonen, P Vainikainen, C Oestges, Non-stationary narrowband MIMO inter-vehicle channel characterization in the 5 GHz band. IEEE Trans. Veh. Technol. **59**(4), 2007–2015 (2010)
12. A Alonso, A Paier, T Zemen, N Czink, F Tufvesson, in *Communications Workshops (ICC), 2010 IEEE International Conference on*. Capacity evaluation of measured vehicle-to-vehicle radio channels at 5.2 GHz (Cape Town, 23–27 May 2010), pp. 1–5
13. H Mousavi, B Khalighinejad, B Khalaj, in *Wireless Communications and Mobile Computing Conference (IWCMC), 2013 9th International*. Capacity maximization in MIMO vehicular communication using a novel antenna selection algorithm (Sardinia, 1–5 July 2013), pp. 1246–1251
14. M Matthaiou, D Laurenson, C-X Wang, in *Wireless Communications and Networking Conference, 2008. WCNC 2008 IEEE*. Capacity study of vehicle-to-roadside MIMO channels with a line-of-sight component (Las Vegas, NV, 3 April 2008 31 March), pp. 775–779
15. A Paier, J Karedal, N Czink, H Hofstetter, C Dumard, T Zemen, F Tufvesson, C Mecklenbrauker, A Molisch, in *Personal, Indoor and Mobile Radio Communications, 2007. PIMRC 2007. IEEE 18th International Symposium on*. First results from car-to-car and car-to-infrastructure radio channel measurements at 5.2 GHz (Athens, 3–7 September 2007), pp. 1–5
16. L Cheng, B Henty, D Stancil, F Bai, P Mudalige, Mobile vehicle-to-vehicle narrow-band channel measurement and characterization of the 5.9 GHz dedicated short range communication (DSRC) frequency band. IEEE J. Sel. Areas Commun. **25**(8), 1501–1516 (2007)
17. G Grant, Rayleigh fading multi-antenna channels. J. Appl. Signal Process. **2002**(3), 316–329 (2002)
18. H Shin, JH Lee, Capacity of multiple-antenna fading channels: spatial fading correlation, double scattering, and keyhole. IEEE Trans. Inf. Theory. **49**(10), 2636–2647 (2003)
19. M Chiani, M Win, A Zanella, On the capacity of spatially correlated MIMO Rayleigh-fading channels. IEEE Trans. Inf. Theory. **49**(10), 2363–2371 (2003)
20. S Jin, X Gao, X You, On the ergodic capacity of rank-1 Ricean-fading MIMO channels. IEEE Trans. Inf. Theory. **53**(2), 502–517 (2007)
21. M Kang, M-S Alouini, Capacity of MIMO Rician channels. IEEE Trans. Wirel. Commun. **5**(1), 112–122 (2006)
22. P Driessen, G Foschini, On the capacity formula for multiple input-multiple output wireless channels: a geometric interpretation. IEEE Trans. Commun. **47**(2), 173–176 (1999)
23. D Gesbert, DGORE H Bolcskei, A Paulraj, Outdoor MIMO wireless channels: models and performance prediction. IEEE Trans. Commun. **50**(12), 1926–1934 (2002)
24. M Matthaiou, P de Kerret, G Karagiannidis, J Nossek, Mutual information statistics and beamforming performance analysis of optimized LOS MIMO systems. IEEE Trans. Commun. **58**(11), 3316–3329 (2010)
25. I Sarris, A Nix, Design and performance assessment of maximum capacity MIMO architectures in line-of-sight. IEEE Proc. Commun. **153**(4), 482–488 (2006)
26. F Bohagen, P Orten, G Oien, in *Wireless Communications and Networking Conference, 2005 IEEE*. Construction and capacity analysis of high-rank line-of-sight MIMO channels, vol. 1 (New Orleans, Louisiana, USA, 13–17 March 2005), pp. 432–437
27. I Sarris, A Nix, Design and performance assessment of high-capacity MIMO architectures in the presence of a line-of-sight component. IEEE Trans. Veh. Technol. **56**(4), 2194–2202 (2007)
28. F Bohagen, P Orten, G Oien, Design of optimal high-rank line-of-sight MIMO channels. IEEE Trans. Wirel. Commun. **6**(4), 1420–1425 (2007)
29. M Ozdemir, H Arslan, Channel estimation for wireless OFDM systems. IEEE Commun. Surv. Tutorials. **9**(2), 18–48 (2007)
30. P Tan, N Beaulieu, A comparison of DCT-based FDM and DFT-based OFDM in frequency offset and fading channels. IEEE Trans. Commun. **54**(11), 2113–2125 (2006)
31. H N Al-Dhahir, S Minn, Satish, Optimum DCT-based multicarrier transceivers for frequency-selective channels. IEEE Trans. Commun. **54**(5), 911–921 (2006)
32. L Han, B Wu, in *Wireless Communications and Signal Processing (WCSP), 2010 International Conference on*. DCT-based channel estimation for wireless OFDM systems with the hexagonal pilot pattern (Suzhou, China, 21–23 October 2010), pp. 1–5
33. F Farrokhi, A Lozano, G Foschini, in *Personal, Indoor and Mobile Radio Communications, 2000. PIMRC 2000. The 11th IEEE International Symposium on*. Spectral efficiency of wireless systems with multiple transmit and receive antennas, vol. 1 (London, 373)
34. F Farrokhi, A Lozano, G Foschini, R Valenzuela, Spectral efficiency of FDMA/TDMA wireless systems with transmit and receive antenna arrays. IEEE Trans. Wirel. Commun. **1**(4), 591–599 (2002)
35. C Shannon, A mathematical theory of communication. Bell Syst. Technol. **27**, 379–423 (1948)
36. J Winters, On the capacity of radio communication systems with diversity in a Rayleigh fading environment. IEEE J. Sel. Areas Commun. **5**(5), 871–878 (1987)
37. A Toding, M Khandaker, Y Rong, Joint source and relay design for MIMO multi-relays systems using projected gradient approach. EURASIP J. Wirel. Commun. Netw. **2014**(155), 1–22 (2014)
38. J Kermoal, L Schumacher, K Pedersen, P Mogensen, F Frederiksen, A stochastic MIMO radio channel model with experimental validation. IEEE J. Selected Areas Commun. **20**(6), 1211–1226 (2002)
39. P Kyritsi, D Chizhik, Capacity of multiple antenna systems in free space and above perfect ground. IEEE Commun. Lett. **6**(8), 325–327 (2002)
40. J Wu, Y Zheng, Oversampled orthogonal frequency division multiplexing in doubly selective fading channels. IEEE Trans. Commun. **59**(3), 815–822 (2011)
41. B-S Y-S Lee, OFDM Seo, receivers using oversampling with rational sampling ratios. IEEE Trans. Consum. Electron. **55**(4), 1765–1770 (2009)
42. D McNamara, M Beach, P Fletcher, P Karlsson, Capacity variation of indoor multiple-input multiple-output channels. Electron. Lett. **36**(24), 2037–2038 (2000)